Supplemental Figure Ⅶ

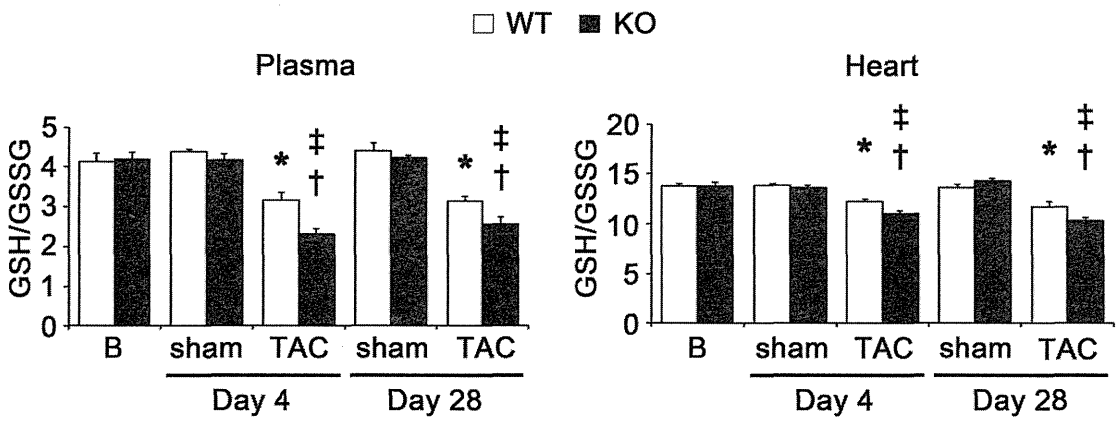

Supplemental Figure Ⅷ

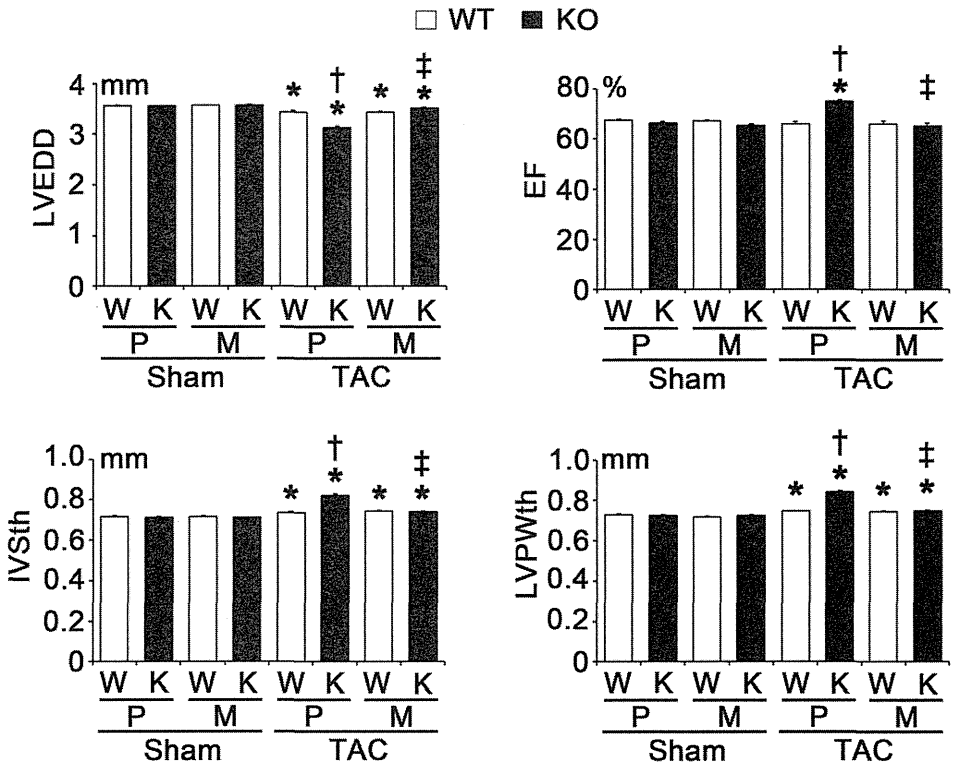

Supplemental Figure IX

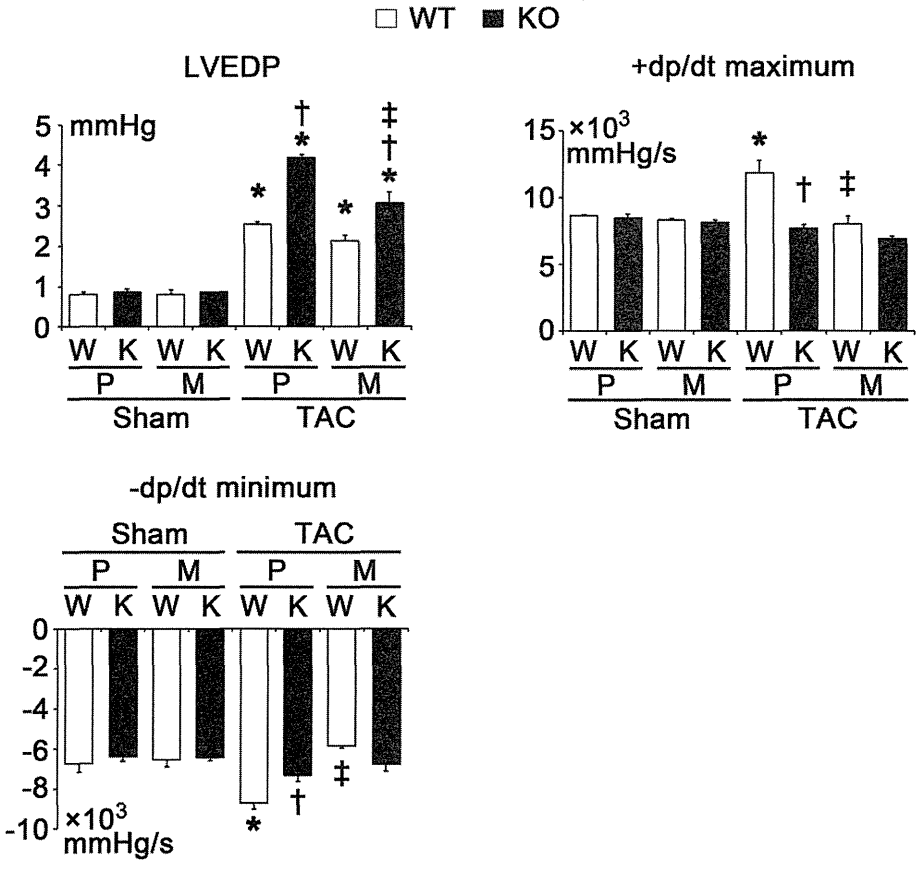

Supplemental Figure X

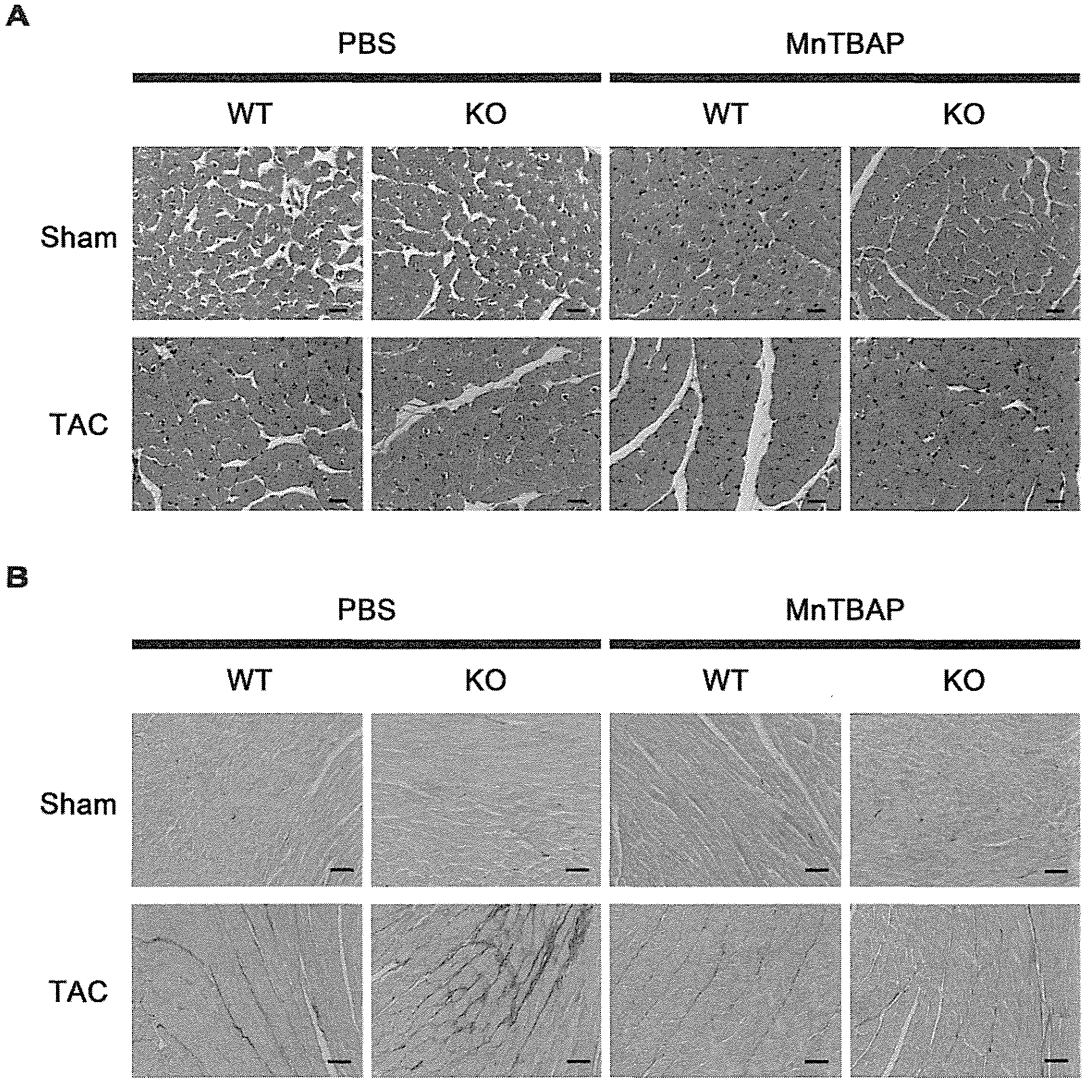

Supplemental Figure XI

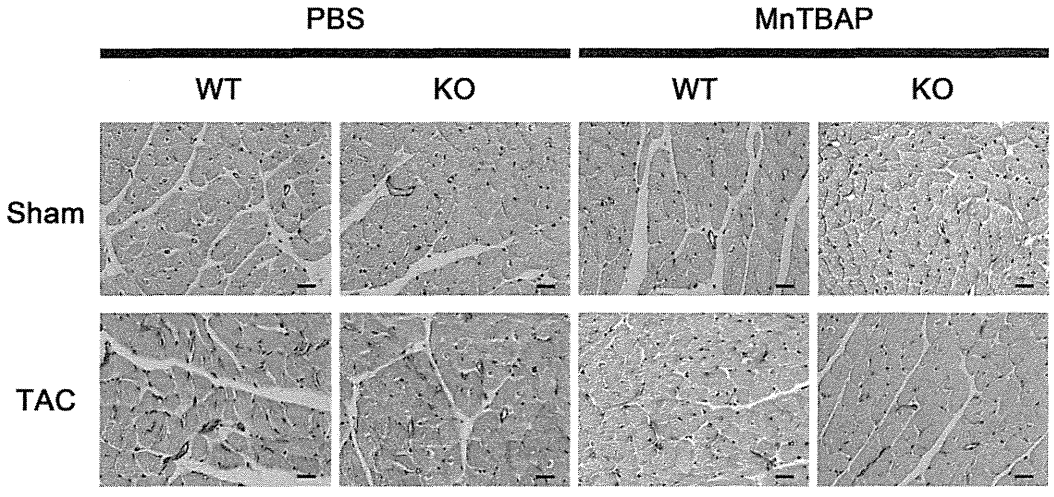

Supplemental Figure XII

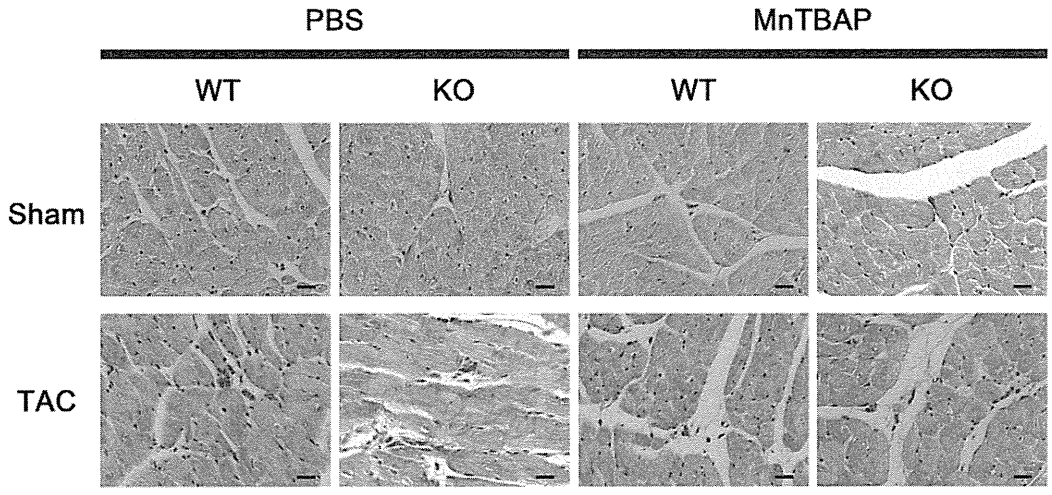

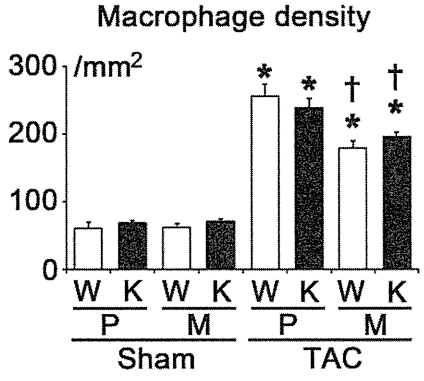

Circulating Transforming Growth Factor β-1 Level in Japanese Patients With Marfan Syndrome

Naomi OGAWA,[1] MD, Yasushi IMAI,[1] MD, Hiroshi NISHIMURA,[1] MD, Masayoshi KATO,[1] MD, Norifumi TAKEDA,[1] MD, Kan NAWATA,[2] MD, Tsuyoshi TAKETANI,[2] MD, Tetsuro MOROTA,[2] MD, Shinichi TAKAMOTO,[2] MD, Ryozo NAGAI,[1,3] MD, *and* Yasunobu HIRATA,[1] MD

SUMMARY

Marfan syndrome (MFS) is an inherited connective tissue disorder mainly caused by the fibrillin-1 mutation. Deficient fibrillin-1 is thought to result in the failed sequestration of transforming growth factor β (TGFβ) and subsequent activation of the TGFβ signaling pathway, suggesting that the circulating TGFβ level may be elevated in MFS, although its accurate measurement is complex due to *ex vivo* release from platelet stores upon platelet activation. We measured the plasma TGFβ1 levels of 32 Japanese MFS patients (22 medically untreated, 10 treated, 20 males, 30.1 ± 9.6 years old) and 30 healthy volunteers (19 males, 29.5 ± 5.8 years old) by ruthenium-based electrochemiluminescence platform (ECL). PF4 was also measured by enzyme immunoassay (EIA) as a platelet degranulation marker. There was no significant difference in the mean plasma TGFβ1 level between the MFS group (1.31 ± 0.40 ng/mL) and controls (1.17 ± 0.33 ng/mL) ($P = 0.16$, NS). Also, there was no significant difference between the untreated (1.24 ± 0.37 ng/mL) and treated (1.46 ± 0.45 ng/mL) MFS patients ($P = 0.15$, NS). We also measured PF4, which showed wide deviations but no significant difference between the two groups ($P = 0.50$). A difference in circulating TGFβ1 levels between MFS patients and controls was not detected in this Japanese population. Circulating TGFβ1 is not a diagnostic and therapeutic marker for Japanese MFS patients, although our findings do not eliminate the possible association of TGFβ with the pathogenesis of MFS. (Int Heart J 2013; 54: 23-26)

Key words: Aortic aneurysm, Aortic dissection, Connective tissue disease, Adult congenital disease, Fibrillin-1

Marfan syndrome (MFS, OMIM #154700) is an autosomal dominant heritable disorder of connective tissue with prominent involvement of the cardiovascular, ocular, and skeletal systems. MFS is caused by mutations of the fibrillin-1 gene (*FBN1*) at 15q21.1[1] that encodes the cysteine-rich, extracellular matrix glycoprotein fibrillin-1(FBN1), which is the major structural component of 10 nm microfibrils. Cardiovascular phenotype is the most important phenotype because it is often related to life-threatening events such as aortic dissection and aneurysmal rupture.[2]

Initially, because FBN1 is a structural element of the extracellular matrix, it was believed a mutation in this gene or changes in its character or amount would bring about structural problems in the vasculature. However, it has subsequently been discovered that changes in FBN1, due to binding of the cytokine TGFβ to FBN1, are correlated to cytokine abnormalities. This is thought to be one important aspect of the pathophysiology of MFS. The TGF cytokines are secreted as large latent complexes, consisting of TGFβ, latency-associated peptide, and one of three latent TGFβ binding proteins. On secretion, the large latent complex is sequestered by the extracellular matrix that includes FBN1. It is hypothesized that deficient or abnormal fibrillin-1 leads to failed sequestration of TGFβ and causes dysregulation of the TGFβ signaling cascade.

Several lines of evidence from the analyses of genetically-engineered mice support an additional role for FBN1 as a regulator of the cytokine TGFβ. Mice homozygous for a hypomorphic *FBN1* allele have impaired pulmonary alveolar septation associated with increased TGFβ signaling that can be prevented by perinatal administration of a polyclonal TGFβ neutralizing antibody.[3] Similarly, myxomatous changes in the mitral valve[4] in mice harboring a *FBN1* missense mutation and aortic aneurysm[5] in mice heterozygous for an *FBN1* allele encoding a cysteine substitution C1039G are attenuated by TGFβ neutralizing antibody or losartan, an angiotensin II type 1 receptor blocker. Additional clinical evidence for this mechanism was provided by Ahimastos' report in which the ACE inhibitor perindopril reduced both aortic stiffness and aortic root diameter in MFS patients and, in addition, both the active and latent forms of plasma TGF-β were remarkably reduced by perindopril administration.[6] In addition, an angiotensin II type 1 receptor blocker, which may attenuate the TGFβ signaling

From the Departments of [1] Cardiovascular Medicine and [2] Cardiothoracic Surgery, Graduate School of Medicine, The University of Tokyo, Tokyo, and [3] Jichi Medical University, Tochigi, Japan.

This work was supported by Health Labor Science's Research Grants from the Japanese Ministry of Health, Labor, and Welfare (YH), and the Funding Program for World-Leading Innovative R&D on Science and Technology (FIRST) from the Japan Society for the Promotion of Science (RN).

Address for correspondence: Yasunobu Hirata, MD, Department of Cardiovascular Medicine, Graduate School of Medicine, The University of Tokyo, 7-3-1 Hongo, Bunkyo-ku, Tokyo 113-8655, Japan.

Received for publication August 9, 2012.
Revised and accepted November 5, 2012.

pathway, significantly reduced the rate of aortic dilation in a small cohort study of MFS children.[7]

Taken together, these findings suggest that the dysregulation of TGFβ, which is an autocrine and paracrine growth factor with involvement in a wide range of biological processes, contributes to the multisystem pathogenesis of MFS. From the above findings, we believe that the level of circulating TGFβ may be elevated in MFS and might reflect the clinical severity and manifestations. However, the accurate measurement of circulating TGFβ1 is complex due to *ex vivo* release of TGFβ1 from platelet stores upon platelet activation. To avoid misevaluation, it is necessary to determine markers for platelet degranulation such as platelet factor 4 (PF4) simultaneously with TGFβ1.

The objective of this study was to examine the circulating TGFβ1 level in Japanese patients with MFS to determine whether it can be used as a diagnostic marker and if it can reflect the pathological role of the TGFβ pathway in MFS.

Methods

Patients: Thirty-two consecutive MFS patients who visited the Marfan clinic at the University of Tokyo Hospital and fulfilled the Ghent criteria (20 males, age range 17-50, 30.1 ± 9.6 years old) and 30 healthy volunteers (19 males, age range 21-45, 29.5 ± 5.8 years old) were enrolled. All patients were assessed using the Ghent criteria.[8,9] Twenty-two of the MFS patients were untreated and 10 were treated with either an angiotensin II type 1 receptor blocker (ARB) or a beta-blocker, or both. All of the control subjects were without any known diseases and were not taking any medications.

This study was conducted according to the Declaration of Helsinki and was approved by the Ethics Committee of the Graduate School of Medicine, The University of Tokyo. Written informed consent was obtained from all the participants after providing a detailed explanation of the study.

Plasma total TGFβ1 measurement in MFS patients: Blood was drawn using a syringe with a 21G needle from a cubital vein and 5 mL was transferred to a tube containing EDTA2Na and immediately placed in iced water and kept for 15 to 30 minutes. Samples were centrifuged at 3000 g for 15 minutes at 4°C. Plasma samples were immediately frozen at -80°C and stored until further analysis.

The plasma total TGFβ1 level in each patient was assayed using a ruthenium-based electrochemiluminescence platform (Meso Scale Discovery, Gaithersburg, MD, USA) according to the manufacturer's protocol. TGFβ1 samples were first acid-activated (with 1N HCl) before assaying. All samples were run in duplicate in this assay. This assay system covers concentrations from 0.1 to 10 ng/mL, and the cumulative interassay coefficient of variation was 14.1%.

Platelet activation greatly affects the results of TGFβ1 measurement. The level of platelet factor 4, which reflects the degree of platelet activation, was also evaluated by enzyme immunoassay (Roche Diagnostics, Japan) according to the manufacturer's protocol at the same time as ELISA assay.

Statistical analysis: Continuous variables are expressed as the mean ± standard deviation (SD). Comparisons of means were performed using the Mann-Whitney *U* test for unpaired values; the correlation coefficient was calculated. All analyses were performed using SPSS software (SAS Institute, USA). A value of $P < 0.05$ was considered significant.

Results

Patient characteristics: All of the MFS patients had aortic root dilatation or a history of cardiovascular surgery including aortic root. Almost 69% of the patients had a positive family history for MFS. We have not done genetic analysis for all the MFS patients, however, 76% of the genetic analyses we have completed have *FBN1* mutations. Skeletal phenotypes were observed in about two thirds of the MFS subjects. Ectopia lentis, pneumothorax, and dural ectasia were also frequently found in the MFS patients (Table).

Circulating total TGFβ1 level in Marfan syndrome: The total TGFβ1 level measured by the ECL platform was 1.31 ± 0.40 ng/mL in the MFS group and 1.17 ± 0.33 ng/mL in the control group, and the difference was not statistically significant (P = 0.16) (Figure 1). When confined to the MFS patients, it was 1.24 ± 0.37 ng/mL in the untreated group and 1.46 ± 0.45 ng/mL in the treated group (P = 0.15) and the difference was not statistically significant (Figure 1). In the MFS patients we evaluated whether there are correlations between the TGFβ1 concentration and clinical severity/phenotypes, however, we did not detect any significant associations.

The PF4 level was also measured at the same time. The concentration of PF4 varied considerably among the individuals in each group. The concentration was 18.34 ± 20.01 ng/mL in the MFS group and 15.30 ± 15.04 ng/mL in the control group, and there was no significant difference between the two groups (P = 0.503) (Figure 2). Among the MFS patients, the concentration was 19.86 ± 20.42 ng/mL in the untreated group and 15.00 ± 19.71 ng/mL in the treated group, which also indicated there was no significant difference (P = 0.533)(Figure 2).

Discussion

In our study the circulating TGFβ1 level was not elevated

Table. Clinical Characteristics of the Patients With Marfan Syndrome

	Total	Untreated	Treated
Number	32	22	10
Male/Female	20/12	15/7	6/4
Age (years)	30.1 ± 9.6	27.8 ± 8.7	35.2 ± 10.1
Cardiovascular			
Aortic root dilatation	32	22	10
History of aortic surgery	3	2	1
Skeletal			
Major criteria, satisfied	9	6	3
Minor criteria, satisfied	13	9	4
Ectopia Lentis	14	9	5
Pneumothorax	14	11	3
Skin lesion	22	15	7
Dural ectasia	18	15	3
Family History	22	13	9
FBN1 mutation	13/17	6/9	7/8
ARB		-	7
Beta Blocker		-	6

ARB indicates angiotensin II type 1 receptor blocker.

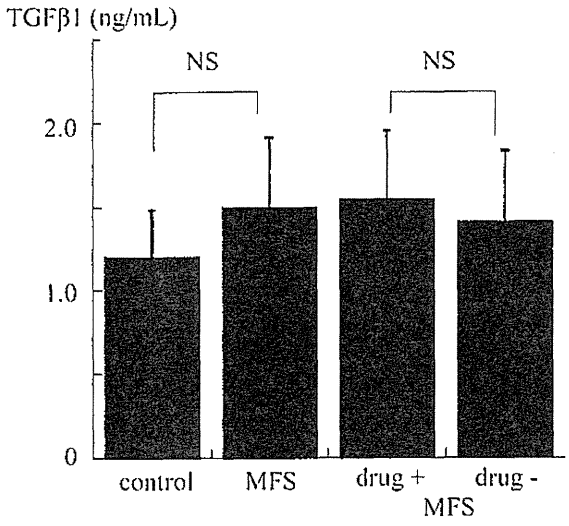

Figure 1. Comparison of TGFβ1 concentration measured by ECL. There was no significant difference between the control subjects and the total MFS patient population. There was also no significant difference in the comparison between the MFS patients with or without medications. NS indicates not significant.

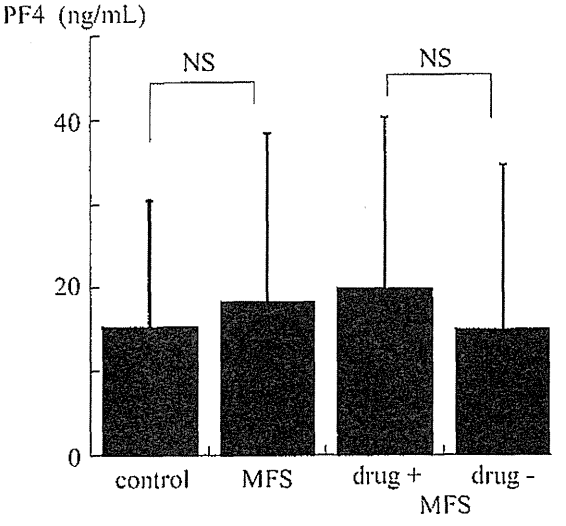

Figure 2. Comparison of PF4, indicative for platelet activation. There was no significant difference between the control subjects and the total MFS patient population. There was also no significant difference in the comparison between the MFS patients with or without medications. NS indicates not significant.

in the MFS patients compared to the control group. While we were preparing and conducting our study, Matt, *et al* reported that the mean TGFβ1 level of MFS patients was about 6 times higher than control subjects in the GenTAC population, although they did not evaluate PF4 level along with TGFβ1, and their sampling scheme was not homogeneous since it was a multicenter study.[10] There was a large discrepancy in the circulating TGFβ1 levels of MFS patients between their report and our study. This difference may be partially due to racial and ethnic differences and the smaller number of patients in our study population. However, the TGFβ1 level in their study was 15 ± 1.7 ng/mL [mean ± SEM, $n = 53$], that is, 15 ± 12.4 ng/mL [mean ± SD] when recalculated. Thus, there seems to be a wide range of variation in the TGFβ1 levels in MFS patients in this previous report as well. Ahimastos, *et al*[6] reported latent and active TGFβ1 levels of 17 MFS patients using an ELISA method which showed even higher levels with mean latent TGFβ1 of 59 ng/mL and active TGFβ1 of 46 ng/mL. We also measured our samples using ELISA and showed very low levels which were almost identical to the levels with ECL (data not shown). One important factor that may help explain this discrepancy is the degree of platelet activation between sample collection and TGFβ1 measurements. The accurate measurement of circulating TGFβ1 is complex due to *ex vivo* release of TGFβ1 from platelet stores upon platelet activation. In addition, contamination by platelets can make the TGFβ1 level appear very high. Since some level of platelet contamination and activation will occur even with the best methods for plasma collection, markers for platelet degranulation such as platelet factor 4 should be determined together with TGFβ1. The low TGFβ1 levels in some MFS patients reported in their study and also in our patients make it difficult to use TGFβ1 as a diagnostic marker of MFS.

In contrast, Radonic, *et al*[11] reported very low levels of plasma TGFβ1, which were 124 pg/mL for MFS patients with aortic dilatation and 10 pg/mL for MFS patients with normal aorta using ELISA, and showed large discrepancies from the above studies. Further studies are needed to define the optimal method for plasma TGFβ1 measurement.

They also stated the mean TGFβ1 level in the treated MFS group was lower than in the untreated MFS group, and concluded the difference was due to a medication effect, raising the possibility of using TGFβ1 as a therapeutic marker. However, we did not observe a statistically significant difference in the TGFβ1 level between the treated and untreated MFS patients in our study population. More prospective studies are required to clarify the effects of medication.

Theoretically, the activated (free) TGFβ1 level should increase while the total TGFβ1 level remains the same because it is believed that failed sequestration of TGFβ1 will lead to activation of the TGFβ signal and subsequent TGFβ pathway in MFS. We attempted to measure activated TGFβ1, however, it was difficult due to its significantly low level. Therefore, we can not deny the possibility that the activated TGFβ1 level might be elevated in MFS.

Some of the MFS patients in the above studies[5,6] had very high TGFβ1 levels. We think it is important to identify the specific clinical/genetic factors accounting for the high TGFβ1 levels. One possible factor might be a genetic difference, specifically the presence of a mutation in TGFβ receptor genes rather than in the *FBN1* gene. However, we measured the TGF level in one patient with Loeys-Dietz syndrome with a TGFBR2 deletion mutation. However, the TGFβ1 level remained low (data not shown). Thus, caution is needed when interpreting the circulating TGFβ1 levels in MFS patients at this moment, and further analysis is needed, at least in Japanese and other Asian patients.

Conclusion: Circulating TGFβ1 showed no elevation in our Japanese MFS patients, demonstrating that circulating TGFβ1 is not a diagnostic and therapeutic marker for Japanese MFS patients, although we can not deny the possible association of TGFβ with the pathogenesis of MFS. Further analysis is need-

ed to elucidate the factors that contribute to the high TGFβ1 levels in certain subgroups with MFS and to identify novel clinical indicators for MFS.

Acknowledgments

We would like to express our sincere gratitude to the patients and their families for agreeing to participate in this work and to all the doctors in the Marfan Syndrome Clinic for their valuable advice. We also thank Keiko Hori, Yumiko Fujimaki, and Takako Kawamura for their excellent technical assistance.

References

1. Dietz HC, Pyeritz RE. Mutations in the human gene for fibrillin-1 (FBN1) in the Marfan syndrome and related disorders. Hum Mol Genet 1995; 4: 1799-809. (Review)
2. Devereux RB, Roman MJ. Aortic disease in Marfan's syndrome. N Engl J Med 1999; 340: 1358-9.
3. Neptune ER, Frischmeyer PA, Arking DE, *et al.* Dysregulation of TGF-beta activation contributes to pathogenesis in Marfan syndrome. Nat Genet 2003; 33: 407-11.
4. Ng CM, Cheng A, Myers LA, *et al.* TGF-beta-dependent pathogenesis of mitral valve prolapse in a mouse model of Marfan syndrome. J Clin Invest 2004; 114: 1586-92.
5. Habashi JP, Judge DP, Holm TM, *et al.* Losartan, an AT1 antagonist, prevents aortic aneurysm in a mouse model of Marfan syndrome. Science 2006; 312: 117-21.
6. Ahimastos AA, Aggarwal A, D'Orsa KM, *et al.* Effect of perindopril on large artery stiffness and aortic root diameter in patients with Marfan syndrome: a randomized controlled trial. JAMA 2007; 298: 1539-47.
7. Brooke BS, Habashi JP, Judge DP, Patel N, Loeys B, Dietz HC 3rd. Angiotensin II blockade and aortic-root dilation in Marfan's syndrome. N Engl J Med 2008; 358: 2787-95.
8. De Paepe A, Devereux RB, Dietz HC, Hennekam RC, Pyeritz RE. Revised diagnostic criteria for the Marfan syndrome. Am J Med Genet 1996; 62: 417-26.
9. Roman MJ, Devereux RB, Kramer-Fox R, O'Loughlin J. Two-dimensional echocardiographic aortic root dimensions in normal children and adults. Am J Cardiol 1989; 64: 507-12.
10. Matt P, Schoenhoff F, Habashi J, *et al.* Circulating transforming growth factor ß in Marfan syndrome. Circulation 2009; 120: 526-32.
11. Radonic T, de Witte P, Groenink M, *et al.* Inflammation aggravates disease severity in Marfan syndrome patients. PLoS One 2012; 7: e32963.

Zinc-finger nuclease-mediated targeted insertion of reporter genes for quantitative imaging of gene expression in sea urchin embryos

Hiroshi Ochiai[a], Naoaki Sakamoto[b], Kazumasa Fujita[b], Masatoshi Nishikawa[c], Ken-ichi Suzuki[d], Shinya Matsuura[a], Tatsuo Miyamoto[a], Tetsushi Sakuma[b], Tatsuo Shibata[c], and Takashi Yamamoto[b,1]

[a]Department of Genetics and Cell Biology, Research Institute for Radiation Biology and Medicine, Hiroshima University, Minami-ku, Hiroshima 734-8553, Japan; [b]Department of Mathematical and Life Sciences, Graduate School of Science, Hiroshima University, Higashi-Hiroshima 739-8526, Japan; [c]Laboratory for Physical Biology, RIKEN Center for Developmental Biology, Chuo-ku, Kobe, Hyogo 650-0047, Japan; and [d]Center for Marine Environmental Studies, Ehime University, Matsuyama 790-8577, Japan

Edited by Eric H. Davidson, California Institute of Technology, Pasadena, CA, and approved May 29, 2012 (received for review February 16, 2012)

To understand complex biological systems, such as the development of multicellular organisms, it is important to characterize the gene expression dynamics. However, there is currently no universal technique for targeted insertion of reporter genes and quantitative imaging in multicellular model systems. Recently, genome editing using zinc-finger nucleases (ZFNs) has been reported in several models. ZFNs consist of a zinc-finger DNA-binding array with the nuclease domain of the restriction enzyme FokI and facilitate targeted transgene insertion. In this study, we successfully inserted a *GFP* reporter cassette into the *HpEts1* gene locus of the sea urchin, *Hemicentrotus pulcherrimus*. We achieved this insertion by injecting eggs with a pair of ZFNs for *HpEts1* with a targeting donor construct that contained ~1-kb homology arms and a *2A*-histone *H2B–GFP* cassette. We increased the efficiency of the ZFN-mediated targeted transgene insertion by in situ linearization of the targeting donor construct and cointroduction of an mRNA for a dominant-negative form of *HpLig4*, which encodes the *H. pulcherrimus* homolog of *DNA ligase IV* required for error-prone nonhomologous end joining. We measured the fluorescence intensity of GFP at the single-cell level in living embryos during development and found that there was variation in HpEts1 expression among the primary mesenchyme cells. These findings demonstrate the feasibility of ZFN-mediated targeted transgene insertion to enable quantification of the expression levels of endogenous genes during development in living sea urchin embryos.

live imaging | quantitative biology

The phenotype and behavior of cells are largely determined by the expression levels of thousands of genes (1, 2). In some cases, the expression dynamics of specific genes also affect cell behavior (3). Therefore, to understand the molecular mechanisms of cellular events, it is necessary to quantify the expression of genes and their dynamics at the single-cell level. Techniques for insertion of a reporter gene into a genomic locus of interest and quantitative imaging of the reporter activities have been developed for this purpose (1, 4). By using these techniques in bacteria, yeast, and mammalian cells, it has been reported that a population of genetically identical cells can exhibit extensive cell-to-cell variability in the expression levels of many genes (3–6). However, for multicellular organisms, a universal technique for gene targeting and quantitative imaging has not yet been established in living animals.

Recently, a method for targeted gene editing using engineered zinc-finger nucleases (ZFNs) has been used in *Drosophila* (7), sea urchins (8), zebrafish (9, 10), plants (11), and human cultured cells (12, 13). ZFNs consist of a customized array of zinc-finger domains that bind to a specific DNA sequence and the nuclease domain of the restriction enzyme FokI. When two ZFNs bind to their associated target sequences in the appropriate direction, the nuclease domains dimerize, and a double-stranded break (DSB) is introduced. The ZFN-induced DSB can then be repaired with high efficiency by either homology-directed repair (HDR) or error-prone nonhomologous end joining (NHEJ) repair independently of a DNA template. Therefore, ZFNs can introduce a site-specific insertion or deletion at the DSB site after NHEJ repair (9, 11). Alternatively, ZFNs can produce defined genetic modifications, including the insertion of a reporter gene, near the site of the DSB by HDR using an exogenous targeting donor construct (7, 11). In animals, it has been noted that ZFN-induced DSBs are mainly repaired by NHEJ, and therefore ZFN-mediated targeted gene correction and transgene insertion are considered to be challenging (7, 14).

In the present study, we performed targeted insertion of a *GFP* reporter cassette into the endogenous *HpEts1* locus of the sea urchin, *Hemicentrotus pulcherrimus*, by injecting a pair of ZFNs with a targeting donor construct. The sea urchin embryo, which is transparent, simple, and readily accessible to experimental perturbations, offers a unique opportunity to study the regulation of morphogenesis during early development. In addition, in vivo quantitative imaging methodology at the cellular level has been established by using confocal laser scanning microscopy (CLSM) (15). Using CLSM, we measured the fluorescence intensity of GFP at single-cell resolution in reporter knock-in sea urchin embryos and found that there was variation in HpEts1 expression among primary mesenchyme cells (PMCs). These findings suggest that ZFN-mediated targeted transgene insertion can be used to quantify the expression levels of endogenous genes during development in sea urchin embryos.

Results

Targeted Transgene Insertion into the HpEts1 Locus Using ZFNs. To explore the possibility of inserting a reporter cassette into a genomic site of interest in the sea urchin, *H. pulcherrimus*, we selected the HpEts1L and HpEts1R ZFNs, whose target sites (5′-GGGGTTGACG-3′ and 5′-GATGATGACT-3′, respectively) are located upstream of the stop codon of the *HpEts1* gene responsible for PMC differentiation (16), by bacterial one-hybrid (B1H) and single-strand annealing (SSA) screenings (8) (Fig. 1*A* and Fig. S1). Zygotic expression of the HpEts1 transcription factor, which is encoded by the *HpEts1* gene, is detected in the nuclei of presumptive PMCs at the hatched blastula stage and in PMCs

Author contributions: H.O. and T.Y. designed research; H.O., N.S., K.F., K.S., S.M., T.M., and T. Sakuma performed research; H.O. and M.N. analyzed data; and H.O., T. Shibata, and T.Y. wrote the paper.

The authors declare no conflict of interest.

This article is a PNAS Direct Submission.

[1]To whom correspondence should be addressed. E-mail: tybig@hiroshima-u.ac.jp.

This article contains supporting information online at www.pnas.org/lookup/suppl/doi:10.1073/pnas.1202768109/-/DCSupplemental.

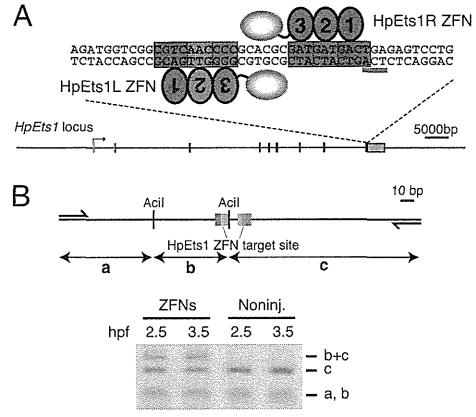

Fig. 1. The HpEts1 ZFNs introduce a DSB at a target site in sea urchin embryos. (*A*) The *HpEts1* gene showing the ZFN target site. A schematic representation of the *H. pulcherrimus* homolog of the *Ets1* gene (*HpEts1*) is shown. Exons are indicated by boxes. The gray and black boxes represent untranslated and coding regions, respectively. The bent arrow depicts the transcription start site. The ZFN-targeted sequence and the interaction site of the pair of ZFNs used in this study are shown. The red bar indicates the stop codon of the *HpEts1* gene. (*B*) Analysis of the mutations induced by ZFNs. A schematic representation of the *HpEts1* genomic region used for the PCR-based analysis is shown in *Upper*. The primer sites are indicated by arrows. The amplified region contains a target site for the HpEts1 ZFNs and two AciI sites. One of the AciI sites is within the HpEts1 ZFN target site. *Lower* shows a representative analysis of the PCR products. The PCR products amplified from genomic DNA extracted at 2.5 and 3.5 hpf from sea urchin embryos injected with the *HpEts1 ZFN* mRNAs (ZFNs) or noninjected control embryos (Noninj.) were purified, digested with AciI, and analyzed by agarose gel electrophoresis.

at the mesenchyme blastula stage (17, 18). To examine the activity of the HpEts1 ZFNs in sea urchin embryos, we amplified the DNA fragments around the target sites for the HpEts1 ZFNs by PCR using genomic DNA extracted from *HpEts1 ZFN* mRNA-injected embryos and control embryos at 2.5 and 3.5 h postfertilization (hpf) and digested with the restriction enzyme AciI (Fig. 1*B*). An AciI-resistant fragment showing the introduction of mutagenesis was observed among the DNA fragments from the *HpEts1 ZFN* mRNA-injected embryos at 2.5 hpf (two- to four-cell stage), and the amount of this fragment was slightly increased at 3.5 hpf (four- to eight-cell stage), indicating that mutagenic NHEJ events occurred after the injection of the *HpEts1 ZFN* mRNAs. These findings suggest that the HpEts1 ZFNs introduced a DSB at their target site as early as 2.5 hpf.

Next, to examine the availability of ZFN-mediated targeted transgene insertion in sea urchin embryos, we prepared two targeting donor constructs, designated Ets-HRD (Fig. 2*A*) and Ets-HRD+T (Fig. 2*B*). The first targeting donor construct, Ets-HRD, contained ~1-kb homology arms and a *2A-H2B-GFP* cassette (2A is a self-cleaving peptide sequence) (19). Therefore, insertion of the reporter cassette into the *HpEts1* locus was expected to result in the expression of two polypeptides: full-length HpEts1 fused with the 17-amino acid sequence of the 2A peptide and H2B–GFP, which localizes to the nucleus where its fluorescence can be accurately quantified (20) (Fig. 2*A*). We confirmed that the 2A peptide mediated protein cleavage in sea urchin embryos by injecting mRNAs for 2A-linked constructs and performing Western blot analyses (Fig. S2). The other targeting donor vector, Ets-HRD+T, contained HpEts1 ZFN target sites at both ends of an Ets-HRD donor cassette and thus generated a linearized targeting donor in the embryos (Fig. 2*B*). In *Drosophila*, it was reported that the efficiency of ZFN-mediated targeted gene modification was increased by using

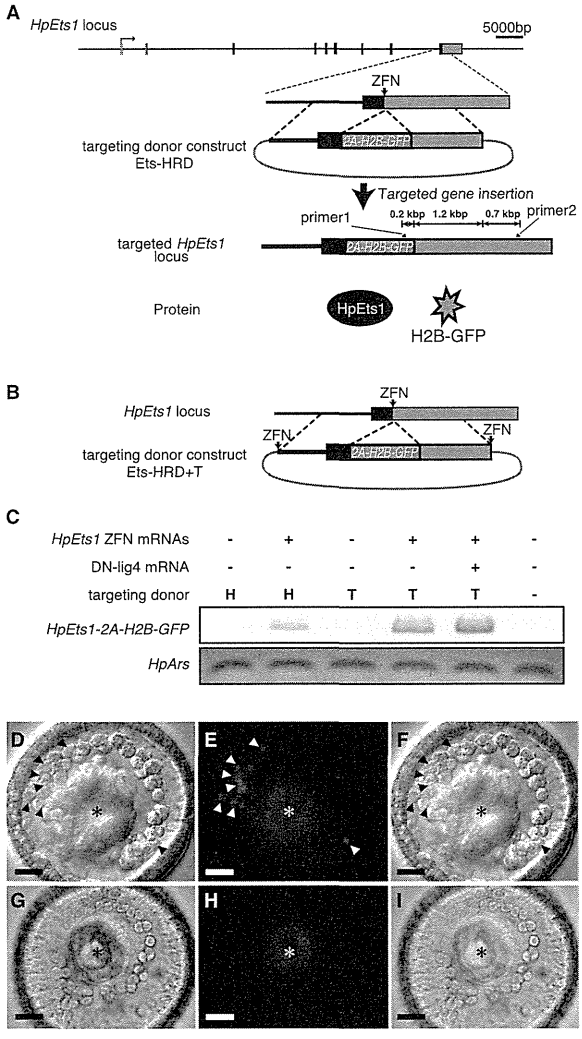

Fig. 2. ZFN-mediated targeted gene insertion. (*A*) Targeting donor construct (Ets-HRD) for insertion of the *2A-H2B–GFP* cassette into the *HpEts1* locus. The structure of the *HpEts1* locus and the targeted *HpEts1* allele are shown. The gray and black boxes represent coding and noncoding exons, respectively. Schematic representations of the proteins derived from the targeted *HpEts1* allele are also shown. These proteins are separated into the full-length HpEts1 protein and H2B–GFP during translation by the 2A self-cleaving peptide. The primer sites for the genomic PCR analysis are indicated. (*B*) Structure of the targeting donor construct Ets-HRD+T, which contains HpEts1 ZFN target sites at both ends of the Ets-HRD cassette. (*C*) Representative results of PCR-based genotyping analysis of the *HpEts1* locus. PCR was performed on genomic DNA extracted from embryos, which had been injected immediately after fertilization at 24 hpf. The primers used were either primers 1 and 2 (as shown in *A*) or primers to amplify the control gene *HpArs*. The PCR products were separated by gel electrophoresis. H and T represent injection of the Ets-HRD and Ets-HRD+T targeting donor constructs, respectively. (*D–F*) GFP-expressing embryo at 30 hpf injected with *HpEts1 ZFN* mRNAs, *DN-lig4* mRNA, and Ets-HRD+T. A representative embryo expressing GFP in the PMCs is viewed from the vegetal pole. (*G–I*) Noninjected control embryo at 30 hpf. (*D* and *G*) Bright field images. (*E* and *H*) Fluorescent images. (*F* and *I*) Merged images of *D* and *E* and of *G* and *H*, respectively. The arrowheads indicate GFP fluorescence in the nuclei of PMCs. Background autofluorescence is denoted by asterisks. (Scale bars, 20 μm.)

an extrachromosomal linear donor, which is linearized in situ, compared with a circular donor (21). In addition, we planned to repress NHEJ repair in the sea urchin embryos. For this purpose,

Table 1. Frequencies of GFP-expressing embryos

Targeting donor construct	*HpEts1 ZFN* mRNAs, each, pg	*DN-lig4* mRNA, pg	Mean GFP-expressing embryos, %*	Mean abnormal embryos, %*
Ets-HRD (40 fg)	—	—	0 (±0)	6.10 (±0.98)
Ets-HRD (40 fg)	1	—	1.86 (±0.60)	10.01 (±1.16)
Ets-HRD+T (40 fg)	—	—	0 (±0)	6.97 (±0.26)
Ets-HRD+T (40 fg)	1	—	12.01 (±0.77)	7.71 (±1.82)
Ets-HRD+T (40 fg)	1	5	15.92 (±1.55)	11.67 (±1.84)

There were three experiments for each targeting donor construct, and in each experiment, 200 embryos were injected.
*Values are mean percentages (averages of all trials) of GFP-expressing and abnormal embryos, respectively, with the SEM in parentheses.

we cloned a cDNA for the carboxyl-terminal tandem BRCT repeat of DNA ligase IV and prepared its mRNA (*DN-lig4*) with the expectation that overexpression of this mRNA would induce a dominant-negative effect, as reported in human cultured cells (22).

To validate the utility of ZFN-mediated targeted transgene insertion in the sea urchin, we injected several combinations of the targeting donor constructs, *HpEts1 ZFN* mRNAs, and *DN-lig4* mRNA, and we then performed PCR analyses using genomic DNA extracted from the embryos at 24 hpf (Fig. 2*C*). As expected, no PCR products were detected in the noninjected and donor-injected samples. In contrast, PCR products of the expected size were observed in the donor/ZFN-coinjected samples and were significantly increased in the Ets-HRD+T/ZFN-coinjected samples compared with the Ets-HRD/ZFN-coinjected samples. Furthermore, the amount of the PCR product was slightly increased in the embryos coinjected with *HpEts1 ZFN* mRNAs, Ets-HRD+T, and *DN-lig4* mRNA compared with those that did not receive *DN-lig4* mRNA. Sequencing of the PCR products confirmed the occurrence of the targeted insertion using the donor constructs (Fig. S3). Next, we examined H2B–GFP expression in the injected embryos using epifluorescence microscopy at 30 hpf (gastrula stage) and counted the numbers of H2B–GFP-expressing embryos (Fig. 2 *D–I* and Table 1). In some embryos, GFP fluorescence was observed in the nuclei of PMCs, in which HpEts1 is expressed (16, 17), and was never detected in other cell types. Consistent with the genomic PCR analysis, GFP-expressing embryos were more frequently observed after injection of Ets-HRD+T, *HpEts1 ZFN*s, and *DN-lig4* mRNAs than after injections with other combinations. These findings suggest that targeted transgene insertion using ZFNs is feasible in sea urchin embryos and that the combined use of donor constructs containing the target sites and DN-lig4 increases the insertion efficiencies.

Quantitative Imaging of Endogenous Gene Expression in Living Sea Urchin Embryos. In sea urchin embryos, in vivo quantification of *GFP* reporter gene expression at the single-cell level has been established by using CLSM (15). We predicted that application of this technique to embryos in which the *GFP* gene was knocked

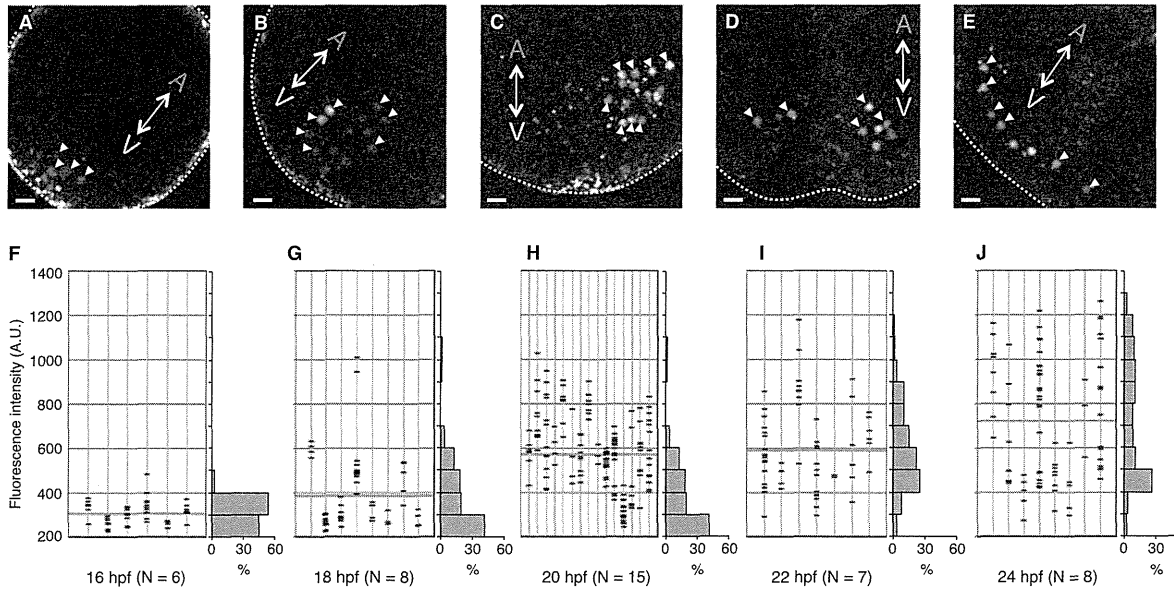

Fig. 3. Quantification of the mean fluorescence intensities in the nuclei of GFP-expressing cells during development. (*A–E*) Projections of *z*-stack images of GFP-expressing embryos. Representative GFP-expressing embryos injected with *HpEts1 ZFN* mRNAs, *DN-lig4* mRNA, and Ets-HRD+T were imaged at 16 (*A*), 18 (*B*), 20 (*C*), 22 (*D*), and 24 (*E*) hpf by using CLSM. The double-headed arrows indicate the animal pole (represented as a red A) and vegetal pole (represented as a green V). The white arrowheads indicate GFP fluorescence in the nuclei of PMCs. The white dotted lines indicate the outside cell surfaces of the embryos. (Scale bars, 10 μm.) (*F–J*) Distributions of the fluorescence intensity of GFP-expressing cells during development. The scatter plots on the left show the distributions of the GFP fluorescence intensities in individual embryos at 16 (*F*), 18 (*G*), 20 (*H*), 22 (*I*), and 24 (*J*) hpf. The orange lines represent the mean fluorescence intensities of GFP-expressing cells at each time point. The histograms on the right show the distributions of the fluorescence intensities of GFP-expressing cells at each time point.

into an endogenous genomic locus would enable real-time quantification of endogenous gene expression. To explore this hypothesis, we imaged embryos injected with Ets-HRD+T, *HpEts1 ZFNs*, and *DN-lig4* mRNAs at 16, 18, 20, 22, and 24 hpf using CLSM (Fig. 3 *A–E*). GFP fluorescence was observed in the nuclei of migrating PMCs at 16 and 18 hpf and in those of PMCs from 18 to 24 hpf. The numbers of GFP-expressing PMCs in the individual embryos ranged from 3 to 43 at 24 hpf (Table S1). Considering that an *H. pulcherrimus* embryo contains 55 ± 10 PMCs at this stage (23), the result suggests that ZFN-mediated targeted transgene insertion occurred at the developmental stage when there were 2–16 PMC-generating cells (Table S1).

As shown in Fig. 3, the mean fluorescence intensity in the cells increased during development. In addition, variation in the fluorescence intensity among cells increased after 18 h (Fig. 3 *F–J*). There are several possible reasons for this observation. First, it may have been caused by variation in the *GFP* copy number, because some GFP-expressing cells may only have had one *GFP* reporter gene monoallelically inserted into the *HpEts1* locus, whereas other GFP-expressing cells may have had two *GFP* reporter genes biallelically inserted into the *HpEts1* locus. To explore this possibility, we coinjected more than 200 fertilized eggs with *HpEts1 ZFNs* and *DN-lig4* mRNA together with Ets-HRD +T and Ets-HRD+mT containing an *mCherry* cDNA instead of the *GFP* cDNA (Fig. S4*A*). We obtained fluorescence images at 24 hpf by CLSM (Fig. S4*B*). In most fluorescent protein-expressing embryos, only one type of fluorescence was observed; 7% and 8% of injected embryos expressed GFP and mCherry, respectively. Although 2% of the embryos possessed both GFP- and mCherry-expressing PMCs, there were no embryos with GFP/mCherry double-positive PMCs. These findings suggest that the reporter construct is monoallelically inserted into the *HpEts1* locus in most fluorescent protein-expressing PMCs. Another possibility is that the variation in fluorescence intensity may have originated from differences in the endogenous HpEts1 expression levels between PMCs. To explore this possibility, we examined the fluorescence intensity of GFP-expressing PMCs and the ingression of PMCs in embryos injected with *HpEts1 ZFN* mRNAs, *DN-lig4* mRNA, Ets-HRD+T, and a moderate dose of an mRNA for a dominant-negative form of HpEts1 (ΔHpEts) (ref. 16; Fig. 4). We expected that the threshold level at which HpEts1 activates PMC differentiation would be raised by the expression of ΔHpEts, which lacks the activation domain and antagonizes native HpEts1 function by blocking its binding to the target site. If the GFP fluorescence intensity is related to the expression level of endogenous HpEts1, we expected that some presumptive PMCs expressing above-threshold levels of HpEts1 and H2B–GFP would differentiate into PMCs, whereas others with below-threshold levels of HpEts1 and H2B–GFP would not migrate into the blastocoel. Consistent with this hypothesis, significantly higher fluorescence intensity was observed in the nuclei of the PMC population than in the other GFP-positive cell population in the blastoderm (Fig. 4). These findings suggest that there is variation in zygotic HpEts1 expression among PMCs.

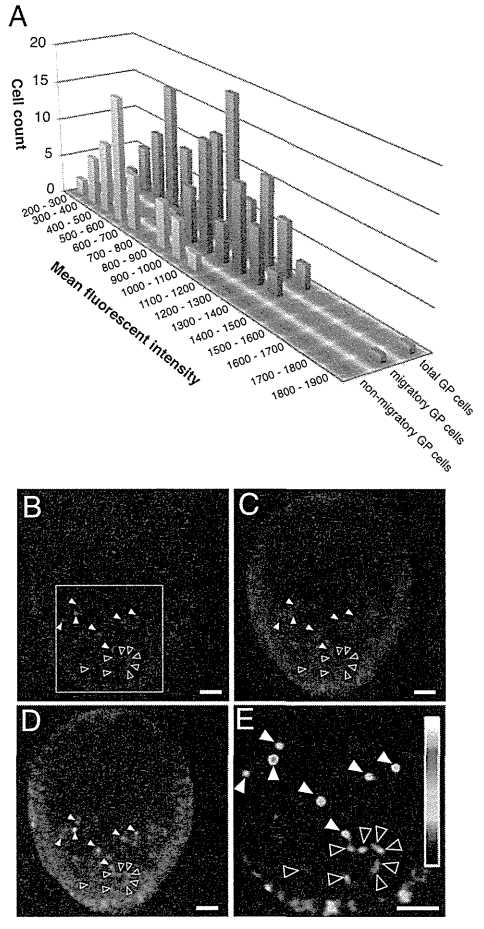

Fig. 4. Variation in fluorescence intensity among GFP-expressing cells. *HpEts1 ZFNs*, *DN-lig4* mRNA, Ets-HRD+T, and *ΔHpEts* mRNA were injected into fertilized eggs, and the fluorescence intensities of GFP-positive cells were quantified at 24 hpf. (*A*) Distribution of the GFP fluorescence intensities in migratory, nonmigratory, or total GFP-positive (GP) cells in embryos injected with a low dose of *ΔHpEts* mRNA. (*B–E*) Representative projections of *z*-stack images of a GFP-expressing embryo coinjected with *ΔHpEts* mRNA. *B*, *C*, and *D* show GFP, Texas Red, and merged images, respectively. (*E*) Pseudocolored and enlarged image of the area marked by the white square in *B*. *Inset* represents the pixel intensity profile. The filled and open arrowheads indicate GFP-positive cells ingressed and not ingressed into the blastocoel, respectively. (Scale bars, 20 μm.)

Discussion

In this study, we have demonstrated that targeted transgene insertion into the *HpEts1* locus can be efficiently achieved by cointroduction of ZFNs and a targeting donor construct in sea urchin embryos. Moreover, by combining this technique with fluorescence quantification, we were able to measure the expression levels of endogenous genes in living sea urchin embryos.

Targeted Transgene Insertion in Sea Urchin Embryos Using ZFNs. Insertion of the reporter gene into the target site was detected in embryos coinjected with the targeting donor construct and *ZFN* mRNAs, but not in embryos injected with the targeting donor alone. These findings indicate that spontaneous homologous recombination is a rare event in the sea urchin embryo and that a ZFN-induced DSB at the target site stimulates HDR, resulting in the induction of targeted transgene insertion at a detectable level. This result is in agreement with earlier work using *Drosophila* and mice (7, 14), suggesting that ZFN-mediated targeted insertion is feasible in model animals, although the efficiency of the insertion may depend on the species. Addition of ZFN target sites at both ends of the targeting donor cassette significantly increased the efficiency of ZFN-mediated targeted transgene insertion. In *Drosophila*, it was reported that an inserted donor was quite inefficient, an excised circular donor was better, and an extrachromosomal linear donor was best for HDR-mediated targeted gene modification (21). Therefore, it is considered that linearization of the targeting donor by ZFNs facilitates DNA strand invasion, which is required for HDR, or stimulates SSA, which involves extensive end processing to reveal complementary single strands in each repeat.

Cointroduction of *DN-lig4* mRNA increased the efficiency of ZFN-mediated targeted transgene insertion. It has been reported that DNA ligase IV, a major component of the NHEJ pathway, forms a complex with XRCC4 and seals DNA ends (22). Moreover, DSB repair can be biased toward HDR by disrupting the function of DNA ligase IV, resulting in an increase in the efficiency of targeted gene modification (7). Therefore, we hypothesized that in the sea urchin, inhibition of DNA ligase IV through the introduction of *DN-lig4* mRNA increases the propensity to repair ZFN-induced DSBs through HDR, resulting in enhanced efficiency of ZFN-mediated targeted transgene insertion. However, in the *Lig4* mutant of *Drosophila*, DSB repair was almost completely biased toward HDR, whereas in the sea urchin, the DN-lig4–mediated enhancement of the efficiency of ZFN-mediated targeted transgene insertion was modest (7). This result may arise because when DSBs are introduced by ZFNs, the DN-lig4 protein is not translated at a sufficiently high rate to completely inhibit the function of the endogenous DNA ligase IV. Therefore, the introduction of recombinant DN-lig4 and ZFN proteins into fertilized sea urchin eggs may enhance the efficiency of ZFN-mediated targeted transgene insertion.

Unintentional off-target cleavages are a potential problem with genome editing using ZFNs (24–26). Potential off-target sites are typically defined by scanning the genome for sites similar to the ZFN recognition sequences. However, because we could not directly search for putative off-target sites, owing to the lack of availability of the *H. pulcherrimus* genomic sequence, we searched for putative off-target sites that contained zero or one mismatches relative to each HpEts1 ZFN target site in the genome of *Strongylocentrotus purpuratus*, which is closely related to *H. pulcherrimus*. We found only one sequence containing one mismatch on *Sp-Ets1/2*, the ortholog of *HpEts1*. This finding implies that the HpEts1 ZFN target site on the *HpEts1* gene is a unique on-target site in the *H. pulcherrimus* genome and that insertion of the reporter gene into other genomic sites is a rare event when HpEts1 ZFNs are used in *H. pulcherrimus* embryos.

Quantitative Imaging of Endogenous Gene Expression in Living Sea Urchin Embryos. We successfully demonstrated visualization of endogenous gene expression in living sea urchin embryos by ZFN-mediated insertion of a *2A-H2B–GFP* cassette into the *HpEts1* locus. In this study, we used the 2A peptide, which is useful for balanced coexpression of multiple proteins from a single promoter, to avoid the synthesis of a fusion protein (19). Although a GFP fusion protein provides subcellular localization information as well as indicates the expression level of the gene of interest (1, 3), GFP may inhibit the function of its fusion partner. In our study, most of the reporter knock-in embryos exhibited normal development, and fluorescent signals were clearly detected in the nuclei of PMCs, suggesting that ZFN-mediated insertion of the *2A-H2B–GFP* cassette is a useful technique for quantitative imaging of gene expression at the single-cell level in developing embryos.

In the present study, we found variation in the expression levels of zygotic HpEts1 among PMCs. However, variation in the amounts of *HpEts1* mRNA and HpEts1 protein has not been detected by standard whole-mount in situ hybridization and immunostaining (16, 18). This variation may arise because these relatively low-sensitivity techniques cannot distinguish subtle variation in the expression levels. Another possibility is that substantial amounts of the *HpEts1* gene product, which was reported to be maternally expressed at abundant levels in whole sea urchin embryos (16), mask the variation in the amounts of the zygotic *HpEts1* gene product. In the latter case, it is difficult to distinguish between maternal and zygotic expression by conventional methods. In fact, although *HpEts1* mRNA is maternally expressed at abundant levels in the whole embryo during early development (16) and the mRNA and HpEts1 protein can be detected in presumptive PMCs and PMCs from the hatching blastula stage, it remains unclear whether this expression pattern is because of zygotic expression of HpEts1, selective degradation of maternal gene products except in presumptive PMCs and PMCs, or both. Therefore, ZFN-mediated reporter insertion is a useful technique for detecting the zygotic expression of an endogenous gene of interest. Our findings also show that PMC differentiation depends on the expression levels of zygotic HpEts1, suggesting that if maternal *HpEts1* mRNA and maternal HpEts1 protein remain in PMCs, they are functionally negligible. Further investigations are needed to understand the biological relevance of the variation in the zygotic HpEts1 expression levels among PMCs.

In most model animals, including the sea urchin, conventional transgenic methods, such as introduction of a reporter construct containing a *cis*-regulatory element of genes into embryos, are carried out to analyze the regulatory mechanism for the spatiotemporal expression of genes (27). However, in these methods, the reporter gene is randomly integrated into the genome, and its expression in embryos may be affected by positional effects, depending on the integration site (28). It was reported that the expression levels of some genes are regulated by distal regulatory elements (29). Therefore, it is uncertain whether sufficient regulatory elements required for endogenous expression are contained in the reporter constructs. In addition, the exogenous DNAs introduced into the sea urchin embryo are joined into concatemers, and multiple copies of them become incorporated into the chromosome (30), meaning that the reporter expression level is not always consistent with the endogenous expression level. In contrast, the combination of the ZFN-mediated targeted gene insertion and in vivo quantitative imaging techniques avoids the above-mentioned problems and enables quantification of the endogenous gene expression level in each cell in real time. The combination of ZFN-mediated targeted gene insertion and live imaging can potentially be applied to examine the relationship between the gene expression level in a cell and its fate. For example, it may be useful for elucidating the transfating mechanisms of presumptive blastocoelar cells to PMCs in embryos whose PMCs were depleted at the mesenchyme stage (31). The combined approach described here using sea urchin embryos might be extended to other multicellular model systems, such as nematodes and zebrafish, in which not only fluorescence imaging techniques but also ZFN-mediated genome modification techniques are available (9, 10, 32).

Materials and Methods

ZFNs targeting *HpEts1* were selected by B1H and SSA screenings as described (8); further information is included in *SI Materials and Methods*. Full descriptions of the constructions of the plasmids used in this study and the sea urchin culture conditions, as well as descriptions of the mRNA synthesis and microinjection, PCR-based genotyping assay, and imaging analysis, are detailed in *SI Materials and Methods* and Fig. S5. The sequences of oligonucleotides used in this study are listed in Tables S2 and S3.

ACKNOWLEDGMENTS. We thank Dr. Keith Joung for providing the pST1374 expression vector (Addgene plasmid 13426); Dr. Daniel Voytas for supplying the pc3XB-ZF60, pc3XB-ZF63, pc3XB-ZF64, and pc3XB-ZF70 vectors (Addgene plasmids 13196, 13199, 13200, and 13193, respectively); Dr. Scot Wolfe for providing the pH3U3-mcs reporter vector, pB1H2x2-zif268 plasmid, and USOΔhisBΔpyrFΔrpoZ bacterial strain (Addgene plasmids 12609, 184045, and 18049, respectively); Dr. Masato Kiyomoto for supplying live sea urchins; the Fisheries and Ocean Technology Center, Hiroshima Prefectural Technology Research Institute for supplying seawater; and the Cryogenic Center of Hiroshima University for supplying liquid nitrogen. This work was supported by Grant-in-Aid for Scientific Research on Innovative Areas 2020006 (to T.Y.) and Grant-in-Aid for Japan Society for the Promotion of Science Fellows 09J01990 (to H.O.). H.O. and T. Sakuma are Japan Society for the Promotion of Science Fellows.

1. Huh W-K, et al. (2003) Global analysis of protein localization in budding yeast. *Nature* 425:686–691.
2. Janes KA, et al. (2005) A systems model of signaling identifies a molecular basis set for cytokine-induced apoptosis. *Science* 310:1646–1653.
3. Cohen AA, et al. (2008) Dynamic proteomics of individual cancer cells in response to a drug. *Science* 322:1511–1516.
4. Sigal A, et al. (2006) Variability and memory of protein levels in human cells. *Nature* 444:643–646.
5. Elowitz MB, Levine AJ, Siggia ED, Swain PS (2002) Stochastic gene expression in a single cell. *Science* 297:1183–1186.
6. Raser JM, O'Shea EK (2004) Control of stochasticity in eukaryotic gene expression. *Science* 304:1811–1814.
7. Beumer KJ, et al. (2008) Efficient gene targeting in Drosophila by direct embryo injection with zinc-finger nucleases. *Proc Natl Acad Sci USA* 105:19821–19826.
8. Ochiai H, et al. (2010) Targeted mutagenesis in the sea urchin embryo using zinc-finger nucleases. *Genes Cells* 15:875–885.
9. Doyon Y, et al. (2008) Heritable targeted gene disruption in zebrafish using designed zinc-finger nucleases. *Nat Biotechnol* 26:702–708.
10. Meng X, Noyes MB, Zhu LJ, Lawson ND, Wolfe SA (2008) Targeted gene inactivation in zebrafish using engineered zinc-finger nucleases. *Nat Biotechnol* 26:695–701.
11. Shukla VK, et al. (2009) Precise genome modification in the crop species Zea mays using zinc-finger nucleases. *Nature* 459:437–441.
12. Urnov FD, et al. (2005) Highly efficient endogenous human gene correction using designed zinc-finger nucleases. *Nature* 435:646–651.
13. Hockemeyer D, et al. (2009) Efficient targeting of expressed and silent genes in human ESCs and iPSCs using zinc-finger nucleases. *Nat Biotechnol* 27:851–857.
14. Meyer M, de Angelis MH, Wurst W, Kühn R (2010) Gene targeting by homologous recombination in mouse zygotes mediated by zinc-finger nucleases. *Proc Natl Acad Sci USA* 107:15022–15026.
15. Damle S, Hanser B, Davidson EH, Fraser SE (2006) Confocal quantification of cis-regulatory reporter gene expression in living sea urchin. *Dev Biol* 299:543–550.
16. Kurokawa D, et al. (1999) HpEts, an ets-related transcription factor implicated in primary mesenchyme cell differentiation in the sea urchin embryo. *Mech Dev* 80: 41–52.
17. Fuchikami T, et al. (2002) T-brain homologue (HpTb) is involved in the archenteron induction signals of micromere descendant cells in the sea urchin embryo. *Development* 129:5205–5216.
18. Yajima M, et al. (2010) Implication of HpEts in gene regulatory networks responsible for specification of sea urchin skeletogenic primary mesenchyme cells. *Zoolog Sci* 27: 638–646.
19. Szymczak AL, et al. (2004) Correction of multi-gene deficiency in vivo using a single 'self-cleaving' 2A peptide-based retroviral vector. *Nat Biotechnol* 22:589–594.
20. Sprinzak D, et al. (2010) Cis-interactions between Notch and Delta generate mutually exclusive signalling states. *Nature* 465:86–90.
21. Beumer K, Bhattacharyya G, Bibikova M, Trautman JK, Carroll D (2006) Efficient gene targeting in Drosophila with zinc-finger nucleases. *Genetics* 172:2391–2403.
22. Wu P-Y, et al. (2009) Structural and functional interaction between the human DNA repair proteins DNA ligase IV and XRCC4. *Mol Cell Biol* 29:3163–3172.
23. Kominami T, Takaichi M (1998) Unequal divisions at the third cleavage increase the number of primary mesenchyme cells in sea urchin embryos. *Dev Growth Differ* 40: 545–553.
24. Gupta A, Meng X, Zhu LJ, Lawson ND, Wolfe SA (2011) Zinc finger protein-dependent and -independent contributions to the in vivo off-target activity of zinc finger nucleases. *Nucleic Acids Res* 39:381–392.
25. Gabriel R, et al. (2011) An unbiased genome-wide analysis of zinc-finger nuclease specificity. *Nat Biotechnol* 29:816–823.
26. Pattanayak V, Ramirez CL, Joung JK, Liu DR (2011) Revealing off-target cleavage specificities of zinc-finger nucleases by in vitro selection. *Nat Methods* 8:765–770.
27. Ochiai H, Sakamoto N, Momiyama A, Akasaka K, Yamamoto T (2008) Analysis of cis-regulatory elements controlling spatio-temporal expression of T-brain gene in sea urchin, Hemicentrotus pulcherrimus. *Mech Dev* 125:2–17.
28. Levis R, Hazelrigg T, Rubin GM (1985) Effects of genomic position on the expression of transduced copies of the white gene of Drosophila. *Science* 229:558–561.
29. Bulger M, Groudine M (2011) Functional and mechanistic diversity of distal transcription enhancers. *Cell* 144:327–339.
30. Hough-Evans BR, Britten RJ, Davidson EH (1988) Mosaic incorporation and regulated expression of an exogenous gene in the sea urchin embryo. *Dev Biol* 129: 198–208.
31. Sharma T, Ettensohn CA (2011) Regulative deployment of the skeletogenic gene regulatory network during sea urchin development. *Development* 138:2581–2590.
32. Morton J, Davis MW, Jorgensen EM, Carroll D (2006) Induction and repair of zinc-finger nuclease-targeted double-strand breaks in Caenorhabditis elegans somatic cells. *Proc Natl Acad Sci USA* 103:16370–16375.

日本小児科学会雑誌　116巻9号　1357～1364（2012年）

原　著

CHARGE症候群26例の臨床的検討

神奈川県立こども医療センター遺伝科[1]，同　内分泌代謝科[2]
石川　亜貴[1]　榎本　啓典[1]　古谷　憲孝[1]　室谷　浩二[2]
朝倉　由美[2]　安達　昌功[2]　黒澤　健司[1]

要　旨

CHARGE症候群（以下CHS）の自然歴を明らかにすることを目的とし，当センターにおけるCHS 26例の出生状況，診断年齢，合併症，医療管理状況，行動特性，就学状況について検討した．

診断年齢は新生児期から24歳までと幅広く，3歳までに約2/3が診断されていた．これまで報告されている合併症の頻度と比べて，後鼻孔閉鎖は30%，食道閉鎖は1例と頻度が低く，口唇口蓋裂は38%と高かった．喉頭軟化症，摂食嚥下障害，胃食道逆流の合併は多く，濃厚な医療管理を必要とする症例が少なくないが，一部は症状が改善し，気管切開や胃瘻の閉鎖が可能となる症例もいた．発達の評価は視覚・聴覚障害のため困難であるが，約8割の症例は手話やジェスチャー・サインなどの手段を使ったコミュニケーションが可能であり，彼らの理解力は実際のパフォーマンスに比べて高いことが推測された．また行動面では，忙しなさや落ち着きのなさが目立つ傾向があり，知的障害の重症度によってその傾向は異なった．早期に視覚・聴覚障害に対する介入，療育を行い，発達の可能性を引き出し，コミュニケーション能力を育てていくことが，精神行動面の安定化，社会性の獲得につながると考えられた．

CHSの合併症，成長発達の特徴，行動特性などの自然歴を，医療，療育，教育の専門家が正しく理解し，個々の患者にあわせて適切な管理を行い生活の質を向上させることが，患者と家族にとって最も重要と考える．

キーワード：CHARGE症候群，合併症，自然歴，発達遅滞，行動特性

はじめに

CHARGE症候群（以下CHS）はコロボーマ（C），先天性心疾患（H），後鼻孔閉鎖（A），成長障害・知的障害（R），外陰部の異常（G），耳の奇形，難聴，内耳奇形（E）を特徴とする多発先天形態異常症候群である．1981年，Pagonらにより疾患概念が確立[1]，2004年に*CHD7*が責任遺伝子として同定され[5]，連合からCHARGE症候群と定義された．*CHD7*遺伝子は分化発生に関与すると考えられている．ほとんどの症例が弧発例で，常染色体優性遺伝形式をとり，発生頻度は1/10,000～12,000出生と推測されているが，最近の報告では，1/8,500人とされている[8]．

CHSの生命予後は合併症の重症度によるが，適切な医療管理がされれば良好である．しかし，合併症が多岐に渡り，多くの専門科にまたがる治療・管理が必須となる．とくに新生児期～乳児期は心疾患の管理，および外科的修復，後鼻孔閉鎖や気道の異常による呼吸障害，哺乳摂取障害の管理（経腸栄養，胃瘻造設）が必要であり，児および家族の不安や負担は大きい．また，Pagonらによって提唱された古典的症状に加えて，近年の医療の経験の蓄積から，脳神経麻痺[7]，内耳異常，視床下部―下垂体障害による内分泌学的異常[18][19]，行動異常[14]～[16]などが児の医療・健康管理上重要であることが示唆されている[20][21]．

このような合併症や医療管理状況，行動特性を含めたCHSの自然歴を明らかにすることは，医療サイドの理解を促し，合併症管理に有用となる．さらに，患者家族へ情報提供をすることにより不安を軽減することが可能となる．今回，我々は当センターでフォローしているCHS 26例について臨床病歴を中心にまとめ，検討を行ったので報告する．

対象および方法

対象は2009年12月現在，当センター通院中もしくは受診歴のあるCHS 26例（男性10例，女性16例）である．診断は臨床症状の組み合わせからVerloes (2005)[6]，Blakeら（1998）[7]の診断基準を参考とし，総合的に臨床遺伝専門医によってなされている．また26

（平成23年6月10日受付）（平成24年2月22日受理）
別刷請求先：（〒006-0041）札幌市手稲区金山1条1丁目
北海道立子ども総合医療・療育センター小児科　石川　亜貴
E-mail: aki.ish.718@gmail.com

表1　CHARGE症候群26例の出生状況，合併症，医療管理

症例	CHD7変異解析	年齢性別	診断年齢	在胎週数	出生体重	コロボーマ	心奇形	後鼻孔閉鎖	体重/身長SD	発達遅滞	外性器低形成性腺機能低下	難聴外耳奇形	消化器系	顔面/反回神経麻痺	口唇口蓋裂	呼吸管理	栄養摂取(最終受診時)	その他の合併症
1	nonsense変異	11/f	5	38	3,030	+	−	−	−2.1/−3.5	+	+	+	−	−/−	CLP	−	経口	側弯，キアリ奇形 精髄空洞症
2	nonsense変異	11/m	1	38	2,426	+	PDA ASD	−	−1.5/−3.1	+ IQ30以下	+	+	−	+/−	−	−	経口	熱性痙攣
3	nonsense変異	13/f	9	39	2,535	+	PDA	+	−2.5/−3.5	+	+	+	−	+/−	−	長期人工呼吸管理 気管切開（3m～9y）	経口＋経腸（胃瘻）	
4	nonsense変異	15/m	10	40	2,598	+	−	−	−3.0/−3.9 GH補充	+ IQ50	+	+	食道閉鎖 GER（ope）	+/+	CP	長期人工呼吸管理	経腸→経口 (14y胃瘻閉鎖)	
5	nonsense変異	18/m	3	40	2,948	+	PDA VSD	−	−1.2/−3	+	+	+ 人工内耳	−	−/−	−	unknown	経口	膀胱尿管逆流 熱性痙攣
6	frame-shift変異	10/m	3	39	3,300	−	−	−	−1.3/−2.1	+	+	+	GER（ope）	+/−	CLP	−	経口＋経腸（胃瘻）	甲状腺機能低下
7	splice-site変異	14/f	2	38	2,778	+	PDA	−	−2.2/−4.1	+ IQ20以下	−	+	GER	+/−	CP	−	経腸→経口(9y～)	側弯
8	missense変異	8/m	1	38	2,686	+	PDA	−	−2.1/−2.7	+	−	+	−	−/−	−	−	経口	甲状腺機能低下 熱性痙攣
9	missense変異	9/m	6	35	1,985	+	ASD	−	−2.4/−4.4 GH補充	+ IQ33	−	+	食道裂孔ヘルニア GER	−/−	CLP	長期人工呼吸管理 気管切開（1～5y）	経腸→経口 (5y胃瘻閉鎖)	
10	missense変異	12/f	5	38	2,650	−	PDA	−	−1.8/−3.8 GH補充	+ 動作性IQ100	−	+	−	−/+	CLP	在宅酸素（0～6m）	経口	
11	変異なし	15/f	13	32	1,452	−	PDA	+	−3.2/−3.8	+	+	+	GER	−/+	−	長期人工呼吸管理（1～5m）披裂粘膜レーザ焼灼	経腸→経口	てんかん 側弯，骨粗鬆症
12	変異なし	28/f	24	40	2,430	+	PDA ECD	−	−2.3/−3.1	+	+	+	−	+/−	CLP	−	経口	脂肪腫
13	解析中	7/f	0	37	2,582	+	PDA VSD	−	−2/−3.3	+	+	+	GER（ope）	−/−	CP	長期人工呼吸管理 気管切開（7m）	経口＋経腸（経鼻）	股関節脱臼，内反足 てんかん，甲状腺機能低下
14	NT	4/f	0	40	2,990	+	PDA	+	−1.4/−3.4	+ IQ47	unknown	+	−	+/−	−	−	経腸→経口(2y～)	
15	NT	5/f	3	38	2,450	+	TGA PDA	−	−3.2/−4.8	+	unknown	+	−	−/+	−	unknown	経腸→経口(3y～)	
16	NT	7/f	0	40	2,592	+	PDA	+	−1.9/−4.7	+ IQ30	unknown	+	GER	−/−	−	長期人工呼吸管理（0～1y）披裂粘膜レーザ焼灼	経腸→経口	膀胱尿管逆流 内頸動脈部分低形成
17	NT	8/m	1	40	3,440	+	DORV PS Ebstein	−	−1.3/−3.8	+ IQ20以下	+	+	GER	−/−	CLP	長期呼吸管理 喉頭気管分離（3y）	経腸（経鼻）	低酸素性虚血性脳症，側弯 てんかん，甲状腺機能低下
18	NT	8/f	1	41	2,878	+	PDA PS Ebstein	+	−2.3/−3.7	+ IQ27	unknown	+	食道裂孔ヘルニア GER（ope）	+/−	−	−	経口＋経腸（経鼻）	側弯，漏斗胸 外傷後てんかん
19	NT	9/m	9	40	3,480	+	−	−	−3.4/−8.0	+	+	+	GER	−/−	−	−	経腸（胃瘻）	
20	NT	13/m	0	41	2,864	+	PDA VSD	+	−0.3/−1	+	+	+	GER（ope）	+/−	CL	−	経口＋経腸（胃瘻）	多指
21	NT	15/f	14	38	3,080	+	Truncus arteriosus	−	−3.1/−4.7	+	+	+	GER	+/−	−	−	経腸→経口(9y～)	
22	NT	18/f	2	38	2,484	−	PDA ASD	−	−2.6/−4.5	+	unknown	+	−	−/−	−	−	経口	側弯
23	NT	20/m	12	38	3,450	+	TOF	−	−2.7/−3.2	+ IQ20以下	+	+	GER	−/−	−	−	経口	側弯
24	NT	20/f	1	40	3,095	−	VSD	+	−1.2/−0.4	+ IQ48	+	+/+	GER	+/−	−	−	経口	側弯，熱性痙攣
25	NT	20/f	7	40	2,550	+	PDA	−	−2.0/−4.2	+ IQ20	unknown	+/+	GER	−/+	−	−	経口	熱性痙攣
26	NT	27/f	3	41	2,650	−	PDA	+	−0.3/1.0	+ IQ48	+	+/+	−	−/+	−	unknown	経口	頸椎癒合肩甲骨形成不全

ASD：atrial septal defect　VSD：ventricular septal defect　PDA：patent ductus arteriosus　ECD：endocardial cushion defect　TOF：tetralogy of Fallot　TGA：transposition of great arteries　DORV：double outlet right ventricle　PS：pulmonary stenosis　GER：gastroesophageal reflux　CLP：cleft lip and palate　CL：cleft lip　CP：cleft palate　NT：not tested

表2 主要な臨床症状の頻度

臨床所見	頻度	
コロボーマ	20/26	77%
心奇形	22/26	84%
後鼻孔閉鎖	8/26	30%
消化器系の異常	3/26	11%
顔面神経麻痺	11/26	42%
口唇口蓋裂	10/26	38%
成長障害	23/26	88%
発達遅滞	26/26	100%
外性器低形成/性腺機能低下	16/19	84%
難聴・外耳奇形	26/26	100%
三半規管 低形成	15/15	100%
嗅球・嗅溝 低形成・無形成	10/10	100%
喉頭軟化症	23/26	88%

例中13例は*CHD7*遺伝子解析を行い，うち10例が変異陽性であった．診療録により後方視的に臨床病歴をまとめ，出生状況，診断年齢，合併症および医療管理状況，行動特性，就学状況について検討した．今回は*CHD7*遺伝子解析を行った症例が半数と少ないため，*CHD7*変異陽性例と陰性例についての遺伝型・表現型の詳細な検討は行っていない．

結　果

26例の出生状況，診断年齢，発達，合併症，医療管理状況については表1に，また臨床所見の頻度については表2にまとめた．最終受診時年齢は7～28歳（中央値：12歳）であった．Verloesの診断基準[6]に従うと典型例が23例，非典型例が3例であった．また26例中13例(典型例11例，非典型例2例)についてCHD7遺伝子解析を行っており，13例中10例にヘテロ接合性変異を認めている．(ナンセンス変異5例，フレームシフト変異1例，スプライシング変異1例，ミスセンス変異3例）残りの3例中，2例は変異を認めず，1例は現在解析中である．*CHD7*変異陽性例10例中，ミスセンス変異例と早期終止コドンをきたす変異例とでは，合併症の頻度や重症度との明らかな相関は認めなかった．

1．診断確定告知年齢

診断が確定し家族に告知された年齢は，新生児期から24歳までと幅広く，その中央値は3歳であった．3歳までに診断されていたのが15例であり，なかには診断が遅れる症例もみられ，就学時以降に診断された症例は8例であった．

2．周産期状況

在胎週数は32～41週（中央値39週），2例が早産であった以外は，ほぼ正期産での出生であった．平均出生体重は2,668g（1,452～3,480）であり，胎児期の成長障害は認めていない．また父親年齢26～46歳(中央値34歳)，母親年齢21～42歳(中央値30歳)であり，一般集団と比べて有意差は認めなかった．

3．臨床症候および医療内容

①循環器疾患

先天性心疾患は22例（84%）に合併し，最も多かったのは動脈管開存17例(動脈管開存単独が9例，他の心奇形との合併が8例）であった．その他は心房中隔欠損症3例，心室中隔欠損症3例，Ebstein奇形2例，ファロー四徴症1例，大血管転位症1例，心内膜床欠損症1例，総動脈管症1例であった．新生児および乳児期に手術を要した症例は22例中15例であった．

②呼吸器疾患

喉頭軟化症は26例中23例（88%）で認めた．新生児期～乳児期にかけて1か月以上の長期呼吸管理を要した症例が7例，喉頭披裂部の異形成に対し披裂粘膜レーザー焼灼が施行された症例が2例，在宅酸素が1例であった．また長期呼吸管理を要した7例中，気管切開術を施行したのは3例で，そのうち2例は呼吸状態が安定し5歳，9歳時に気管切開孔を閉鎖している．また著しい低血糖とショックにより低酸素性虚血性脳症を合併した1例は喉頭気管分離術を施行していた．在宅人工呼吸器管理を行っている症例はなかった．

③消化器疾患

食道閉鎖1例，食道裂孔ヘルニア2例は，いずれも外科的修復(3例全例に胃食道逆流を合併し，2例ではNissen噴門形成術も施行）を要した．胃食道逆流単独で合併したのは10例で，このうち4例がNissen噴門形成術を行っていた．胃瘻造設術が施行されたのは6例で，その内訳は食道閉鎖1例，食道裂孔ヘルニア1例，嚥下障害＋胃食道逆流が3例，残りの1例は胃食道逆流を認めなかったものの，嚥下障害のため長期経管栄養を要し，患者本人の希望で胃瘻管理となった．なお食道閉鎖，食道裂孔ヘルニアで胃瘻を造設した症例は，それぞれ5歳時，14歳時で経口摂取が確立し胃瘻を閉鎖した．

④内分泌疾患[10]

内分泌科の受診歴のある症例は17例であった．低ゴナドトロピン性性腺機能低下（外陰部低形成，思春期遅延を含む）は，評価可能であった19例中16例（男性8例，女性8例)(84%）に認めた．16例中，ホルモン治療を行っているのは男性2例，女性5例の7例であった．また中枢性成長ホルモン分泌不全に対しGH補充を行っている症例が3例，中枢性甲状腺機能低下症にて甲状腺ホルモンの補充を行っている症例は4例であった．

⑤中枢神経系疾患

単純型熱性痙攣5例，てんかん4例の合併を認めた．

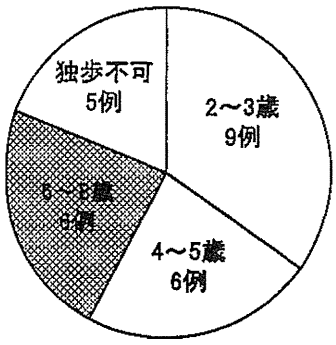

図1　独歩獲得年齢

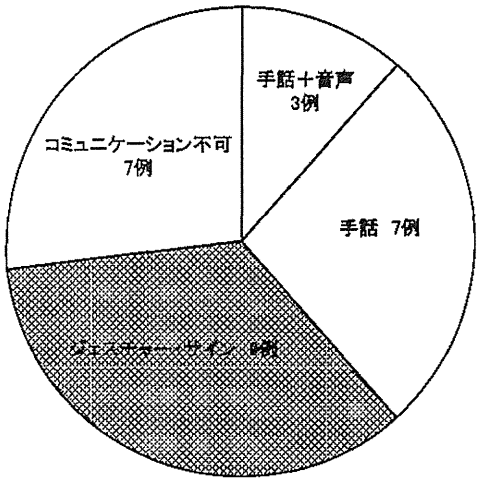

図2　コミュニケーション方法

てんかんの4例のなかには，低酸素性虚血性脳症後遺症1例と頭部外傷後てんかん1例を含んでいた．抗てんかん薬による治療を要した症例はてんかんを合併した4例中3例であった．他の中枢神経系疾患の合併として，キアリI型奇形，脊髄空洞症を1例に認めた．

⑥眼科疾患

全例において眼科精査，および定期受診がなされており，網脈絡膜のコロボーマは20例（77%）に，8例に小眼球を認めた．その他，斜視11例，屈折異常14例，白内障1例の合併を認めた．

⑦耳鼻科疾患

CHSで特徴的な耳介変形(CHARGE ear)，難聴は全例（100%）で認めた．1例のみ難聴が中等度であり補聴器を使用していないが，残りの25例は高度難聴であり，補聴器を使用している．人工内耳の手術が行われたのは，1例のみであった．

後鼻孔閉鎖（狭窄も含む）は8例（30%）に認め，その内訳は後鼻孔閉鎖4例(骨性3例，膜性1例)，後鼻孔狭窄3例，鼻咽腔閉鎖不全1例であった．また滲出性中耳炎の合併も多く24例（92%）で認めていた．

⑧泌尿生殖器疾患

男性10例中，停留精巣の合併は5例(50%)，2例で精巣固定術が施行された．また，膀胱尿管逆流を2例に合併していた．

⑨整形疾患

側弯は8例（30%）に合併していた．その他，骨粗鬆症1例，先天性頸椎癒合，肩甲骨形成不全1例，左臼蓋形成不全1例，漏斗胸(形成手術施行)1例の合併がみられた．

⑩摂食・嚥下障害

全例で嚥下・摂食障害(軽度～重度)を認めていた．哺乳障害はあるものの新生児期から経口摂取のみの症例は8例，新生児～乳幼児期に経腸栄養（胃瘻もしくは経管）を一時的に併用していたが，調査の時点では経口摂取のみであった症例は11例，経口摂取と経腸栄養を併用している症例は5例，経腸栄養のみの症例が2例であった．経口摂取が可能な症例も，嚥下障害，口腔過敏などにより，離乳食への移行が進まず，長期にわたり摂食訓練を行っている症例が多かった．

⑪形成外科疾患

口唇・口蓋裂の合併は10例（38%）であり，全例で修復術が行われた．その内訳は口唇口蓋裂6例，口蓋裂3例，口唇裂1例であった．その他，形成外科的な修復術を要したのは，後鼻孔閉鎖2例，耳介奇形1例，左多指1例であった．

⑫内耳CT（三半規管，斜台の評価)[17]

三半規管，斜台を内耳CTで評価した症例は16例であり，全例で三半規管の低形成もしくは無形成，斜台の低形成を認めた．

⑬頭部MRI（嗅球，嗅溝の評価)[19]

頭部MRIにて嗅球・嗅溝を評価した症例は11例であり，全例で嗅球・嗅溝の低形成を認めた．

⑭成長障害

最終受診年齢時の測定で，体重が－2SDを下回った症例は，26例中15例，身長が－2SDを下回った症例は26例中23例であり，成長障害を認めない症例は3例存在した．体重の平均SD値は－1.9±0.78，身長の平均SD値は－3.2±1.40であった．

⑮精神運動発達，行動特性

独歩獲得年齢の内訳を図1に示す．21例が2～8歳に独歩を獲得していた．5例が独歩未獲得で，このうちの1例は股関節臼蓋不全のため立位は可能であるが歩行は困難で，車椅子を使用している．またもう1例は低酸素脳症後遺症のため痙性四肢麻痺で寝たきりの状態である．また1例はつかまり立ちが可能となった5歳以降，受診歴がなく詳細不明である．残り2例は，8歳，9歳の時点で独歩未であり，運動発達遅滞は重度と思われる．